Essential Readings in Light Metals: Aluminum Reduction Technology.
Edited by Geoff Bearne, Marc Dupuis and Gary Tarcy.

THE DISSOLUTION OF ALUMINA IN CRYOLITE MELTS

J. Thonstad *, A. Solheim *, S. Rolseth * and O. Skar **

* Laboratories of Industrial Electrochemistry and SINTEF, The Foundation for Scientific and Industrial Research at The Norwegian Institute of Technology, 7034 Trondheim, Norway.

** Hydro Aluminium Årdal Verk, 5870 Øvre Årdal, Norway

By means of existing theory for mass and heat transfer to spherical particles the dissolution time for individual alumina grains dispersed in cryolite melts was calculated to be of the order of 10 s, in agreement with experiments. Heat transfer is limiting during heat-up but not during dissolution. Under normal conditions alumina powder agglomerates when being fed to the melt, and lumps are formed which dissolve much more slowly (minutes, hours). An electroanalytical technique was used to monitor the alumina concentration in the bath, and dissolution rates were determined for alumina being fed to the bath as well as for alumina resting at the bottom and for rotating alumina discs. The results were fitted to models for mass transfer controlled reactions.

INTRODUCTION

In the literature there are a large number of experimental studies on the dissolution of alumina in cryolite melts, i.e. in the electrolyte used in Hall-Heroult cells. In spite of the fact that alumina has a fairly high solubility in such melts (~ 10 wt %) the problem of bringing the alumina feed into solution has always been of major concern in the operation of aluminium cells.

The purpose of the numerous experimental studies has been threefold,

- determine the rate controlling step in the dissolution process
- determine the rate of dissolution
- compare dissolution behavior of different aluminas

In the latter case one has been concerned with relationships between rates of dissolution and properties of the aluminas like content of α-Al_2O_3, grain size distribution, LOI, BET surface area, angle of repose etc. Although some attempts have been made in this direction (1,2) much more work will be required to reach final conclusions. As long as the reaction mechanism is not known, it is difficult to predict the dissolution behaviour.

The reason for the present lack of understanding of the alumina dissolution process is to be found in its complexity, as outlined in the following. On the basis of laboratory experiments it may be difficult to simulate what happens in industrial cells. Different alumina feeding techniques used in industrial cells may also set different requirements to the alumina (3).

The Dissolution Process

We assume that the alumina is of the sandy type (low alpha) and that it is "cold" relative to the bath when being added in the form of powder. The dissolution process can be divided into four steps,

1. The alumina hits the surface of the bath and it spreads on the surface. Bath freezes around those grains which are in direct contact with the bath. For a short while a frozen crust is formed while heating occurs, followed by remelting and further wetting. (If enough heat is not available the freezing will persist and a permanent crust is formed).

2. During heating the intermediate crystal modifications of alumina (often called gamma alumina) are converted to alpha alumina, and at the same time sintering occurs (4).

3. When the frozen bath eventually has melted away the alumina grains are partly sintered together (due to 2) forming larger agglomerates or lumps which will tend to sink in the melt.

4. The dissolution process starts as soon as the alumina is exposed to the bath. The dissolution involves strong interaction with the fluoride melt under formation of oxyfluoride species which diffuse away from the interface. The overall dissolution rate will depend on the exposed surface area. This area can vary within several orders of magnitude depending on whether individual alumina grains are dispersed in the melt or whether lumps have been formed. Thus, there are reports in the literature giving dissolution times ranging from a few seconds to several tens of minutes.

Rate Control

The first steps in the dissolution process which involve freezing and melting of bath around the alumina grains, are obviously heat transfer controlled.

During the dissolution (step 4) three rate controlling processes are possible

- heat transfer
- mass transfer
- slow chemical reaction

Apart from the sintering and lump formation (step 2) it is possible to use general theory to elucidate probable mechanisms and dissolution rates.

Mass Transfer. Equations concerning forced convection mass transfer between a fluid and a solid body are usually given as a correlation between the dimensionless Sherwood (Sh), Reynolds (Re) and Schmidt (Sc) numbers. For a sphere, the following equation applies (5)

$$Sh = 2 + 0.6\ Re^{1/2}\ Sc^{1/3} \quad (1)$$

or

$$k \cdot d \cdot \varrho / D = 2 + 0.6\ (\varrho v d_p/\mu)^{1/2} (\mu/\varrho\ D)^{1/3} \quad (2)$$

All symbols are defined in the Appendix. It is also shown that these equations can be applied for falling alumina particles in cryolite.

As can be seen from eq. (1), Sh depends on Re, which can be calculated from the terminal velocity of a particle falling through the melt. For very small Re, i.e. Sh = 2, an analytical solution for the time of dissolution can be obtained

$$t = \varrho_a \cdot d_p^{\ 2}/8D \cdot (C_{sat} - C) \quad (3)$$

as outlined in the Appendix.

For given values of the density (ϱ_a), the diameter (d_p) of the particle and the diffusion coeffcient (D) of alumina dissolved in the melt the time of dissolution is inversely proportional to the difference between the saturation concentration and the bulk concentration of alumina.

Times of dissolution calculated from eq. (3) must be regarded as maximum values, since the approximation Sh = 2 does not hold for free-falling particles with diameters larger than 20 μm (see Appendix). The application of stirring may also give larger particle Reynolds numbers than calculated from the free-fall terminal velocity.

Introduction of numerical values (Appendix) yields t = 4.1 and 16.4 s for 50 μm and 100 μm grain sizes respectively. For particles dispersed in a stirred melt these times will obviously be shorter.

Heat Transfer. Asbjørnsen et al. (6) estimated the time it takes to remelt the frozen bath shell which forms around a cold alumina grain when it enters the bath. For a 100 μm particle the calculated maximum shell thickness was 15.7 per cent of the particle radius and the time for complete remelting was 2.3 s. The heat transfer coefficient used in these caculations (116 W m^2 K) was apparently rather arbitrarily chosen. Likewise, Jain et al. (7) suggested that the individual alumina grains initially would be covered by a protective freeze, and that remelting and dissolution would be limited by heat transfer. Bagshaw et al. (2) calculated that for a heat transfer coefficient (h) of 1200 W/m^2 K the remelting would take about 4-6 s for alumina grains 70-100 μm in diameter. The value of h was adopted from a work by Taylor et al. (8), who carried out experiments where a rod was suddenly immersed into a cryolit melt. This value would be much too low for single grains due to the small dimensions and the spherical shape, as will be shown in the following. However, for larger agglomerates 1200 W/m^2 K may be realistic.

Once the frozen shell has melted away and the particle has reached the bath temperature, the heat requirement corresponds to the endothermic heat of dissolution (at 3 wt % Al_2O_3, ΔH_{diss} = 150 kJ/mol (9)). The heat transfer needed to sustain the dissolution process sets up a temperature gradient so that the temperature at the alumina surface will be lower than the bulk temperature. If this difference gets large it will affect the dissolution rate and become rate determining.

For spherical particles this temperature difference can be estimated. Heat transfer to a sphere can be calculated by an equation similar to eq. (1) (5),

$$Nu = 2 + 0.6\ Re^{1/2}\ Pr^{1/3} \quad (4)$$

or

$$h \cdot d_p/\lambda = 2 + 0.6\ (\varrho v d_p/\mu)^{1/2}\ (C_p \cdot \mu/\lambda)^{1/3} \quad (5)$$

The symbols are explained in the Appendix.

As can be seen from eq. (4), the lowest attainable value for the Nusselt number is 2, which is due to the spherical geometry. Consequently, the heat transfer coefficient to a single grain will at least be in the order of 10^4 W/m^2 K for a grain of 100 μm in diameter. This value is one to two orders of magnitude higher than these used by the previous workers (6,7).

The ratio between the heat flux and the mass flux corresponds to the heat of dissolution, which increases with decreasing alumina concentration (see Table A2)

$$Q/J = h\ (T - T^*)/k\ (c_{sat} - c) = \Delta H_d \quad (6)$$

The ratio between the heat transfer coefficient (h) and the mass transfer coefficient (k) can be found from eqs. (1) and (4). As outlined in the Appendix, this ratio depends on the magnitude of Re. As an example it is shown that for an average value of (c_{sat} - c) = 100 kg m^{-3} the temperature difference (T-T*) between the bulk of the melt and the alumina surface comes out as 2.2 and 0.5 degrees for low and high Reynolds numbers respectively. These low values signify that the dissolution process cannot be heat transfer controlled under normal circumstances.

For melts which are far from saturation (below the eutectic composition) heat transfer control would imply that the surface of the alumina (where the dissolution takes place) is at the temperature at which freezing of bath occurs. If we regard the simple cryolite-alumina eutectic system, this temperature corresponds to the eutectic temperature (T_c) as illustrated in Fig. 1.

We see from the figure that the temperature distance from the liquidus (primary crystallization of cryolite) is shorter for the bulk of the melt (a) than at the surface of the dissolving alumina (b). Hence, freezing of cryolite cannot take place at the surface of the alumina grains during the dissolution process. As calculated above the temperature difference (T - T*) between A and B is small.

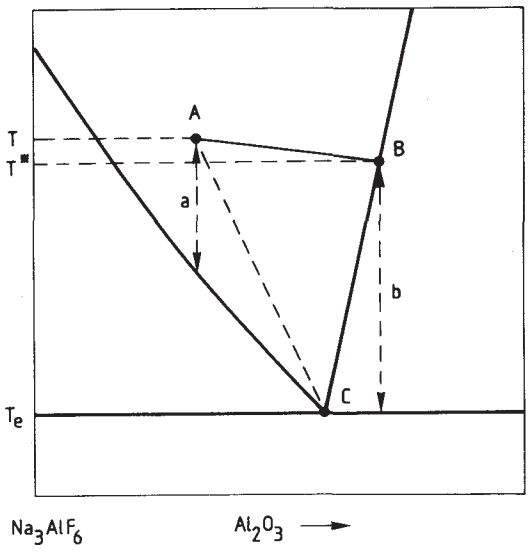

Figure 1 - Sketch of the cryolite-alumina phase diagram. A - An arbitrarily chosen bath temperature (T) and composition. B - surface of dissolving alumina grains at temperature T*. C - eutectic, corresponding to the lowest temperature, T_e, where crystallization of cryolite can occur.

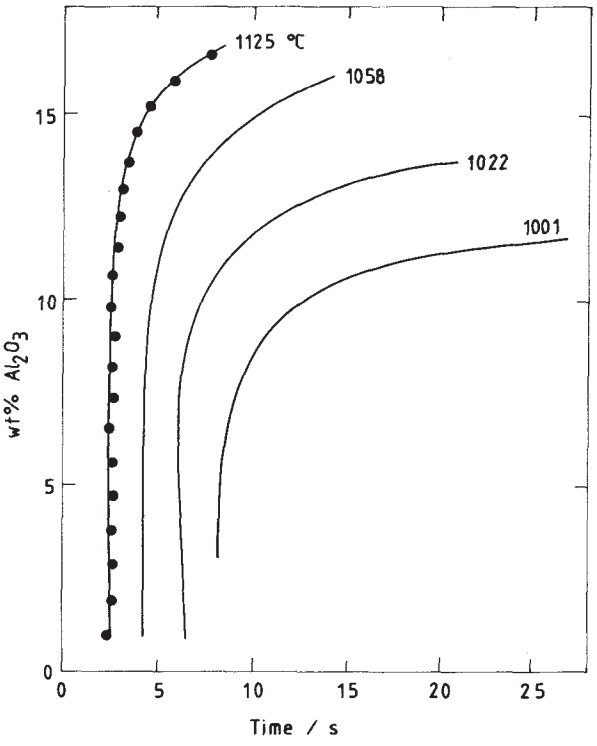

Fig. 2 - Dissolution time (s) for 1 wt % Al_2O_3 which was dispersed in a cryolite melt. The dissolution time was determined visually (10).

Reaction Control. The dissolution of alumina in cryolite involves the disrupture of the alumina lattice and formation of new oxyfluoride species in solution. A slow chemical reaction can therefore not be rejected a priori. It is not possible to estimate the reaction rate for reaction control, but the shape of the concentration-time curve can be predicted if the reaction order is known. It has been suggested that the reaction is of zero order at low alumina concentrations (10,11). The concentration-time curve will then be linear. A first order reaction gives the same shape of the curve as for mass transfer control (see eq. 8)

EXPERIMENTAL AND RESULTS

In the following some experimental data obtained in laboratory experiments will be used to throw light on the dissolution process, in view of the theoretical treatment given above. However, this treatment cannot be applied when agglomeration of the alumina occurs, because the size, shape and life-time of these agglomerates cannot be estimated.

Dissolution of dispersed alumina powder

The experimental conditions which are amenable to the use of the equations cited above would be the study of the dissolution time of individual grains or of batches of alumina which are effectively dispersed in the melt without appreciable agglomeration taking place.

This was assumed to be accomplished by adding batches of 1 wt % alumina to a vigorously stirred melt. The dissolution time was determined by visual observation as the time from the addition was made until the melt became clear again. The results have been reported previously (10), so only one set of curves will be given here, as shown in Fig. 2.

The shape of the curves at low alumina contents seems to indicate a zero order reaction control (10). However, it must be borne in mind that the dissolution time is the sum of the time it takes to heat the alumina (freezing and melting of the cryolite shell) and the time of dissolution. The former will be little dependent on the alumina concentration.

It is not known to what extent the dispersion of the alumina grains was complete. In fact, the shape and the temperature dependence of the curves can also be explained by assuming that small agglomerates (mm size) are formed and that the overall process is governed by heat transfer (melting) and mass transfer (dissolution). If the process is treated as mass transfer controlled, it is seen that the dissolution times are of the same order of magnitude as the theoretical values calculated above. As would be expected the measured times are somewhat shorter.

Rotating Disc Experiments

Several authors (12-14) have studied the rate of dissolution (r) of a rotating disc of sintered alumina in cryolite melts. For a mass transfer controlled process the Levich equation (15) applies

$$r = 0.62\ \omega^{1/2}\ \nu^{-1/6}\ D^{2/3}\ (c_{sat} - c) \qquad (7)$$

where ω is the angular velocity, ν the kinematic viscosity and D the diffusion coefficient.

A commercially available sintercorundum disc of 30 mm diameter was used in these experiments. As shown in Fig. 3 the expected dependency on the angular velocity was observed in agreement with the results of the previous works (12-14). From the slope of the curve the diffusion coefficient was found to be $1 \cdot 10^{-9}$ m^2 s^{-1}. This value is somewhat uncertain since the outer rim of the disc was not shielded. However, the value is of the same order as found by other workers (16).

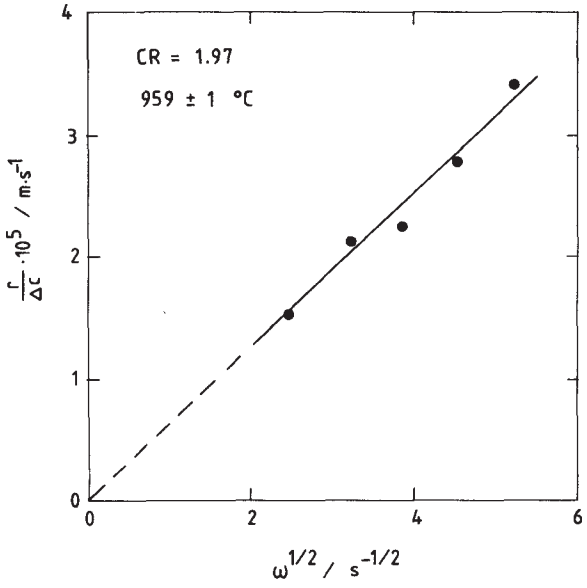

Fig. 3 - Dissolution of a rotating disk of sintered alumina in a melt with molar ratio $NaF/AlF_3 \approx 2$; 950°C.

Dissolution of Alumina in a Melt Kept at its Liquidus Temperature

As illustrated in Fig. 1 freezing of cryolite due to insufficient heat supply should not occur at the surface of the dissolving alumina grains. Such freezing will rather occur out in the bulk of the melt, and the dissolution should proceed even if the melt is kept at its liquidus temperature. When alumina is added to such a melt, the alumina should dissolve and the bulk of the melt should remain at its liquidus temperature. Since the liquidus temperature decreases with increasing alumina content, the temperature of the melt will actually decrease. Cryolite will freeze out to supply some of the heat needed for the dissolution process.

Experiments were performed to test this hypothesis. A cryolite-alumina melt was kept at its liquidus temperature as determined in situ prior to the experiment by recording cooling curves. The melt was vigorously stirred upon addition of batches of 1 wt % Al_2O_3 each. As shown in Fig. 4 the bath temperature very rapidly dropped to its new liquidus temperature after each addition (~ 5° per wt % Al_2O_3). This indicates that the alumina was dissolved readily also in this case.

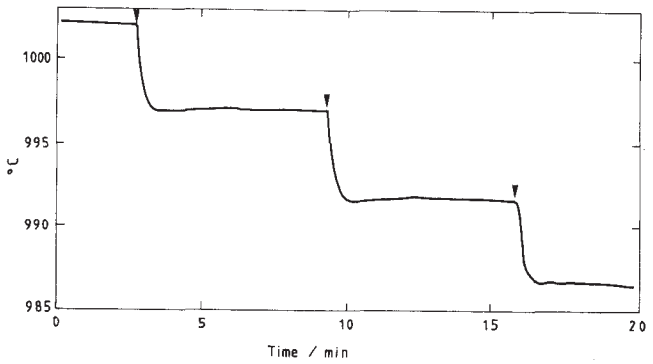

Fig. 4 - Changes in bath temperature by batchwise additions of 1 wt % alumina to a cryolite melt which was kept at its liquidus temperature. Vigorous stirring was applied.

Alumina Resting at the Bottom

The experiments described so far based on vigorous stirring or dissolution of rotating discs do not reflect the conditions prevailing during alumina dissolution in industrial cells. Due to agglomeration and crusting the dissolution tends to be slow, and part of the alumina added settles at the bottom of the cell.

To study the dissolution process in the laboratory the well known critical current density (ccd) measurements were adapted for automatic recordings of the alumina levels every 30 seconds. A graphite electrode dipping into the melt is subjected to a linearly increasing current until a maximum (ccd) is reached, which signals the onset of the anode effect. The ccd increases almost linearly with the alumina content according to calibration curves for the electrode. Similar equipment has previously been described by Jain et al. (1).

In traditional alumina feeding at long intervals (hours) only a small fraction (~ 1/3) of the alumina added dissolves shortly after crustbreak (17). Some of the undissolved alumina will settle in the cell, e.g. along the side ledge where it can remain exposed to the bath. The nature of this material will correspond to that of sludge, i.e. a mixture of alumina and saturated bath.

The dissolution of sludge has been studied by keeping sludge at the bottom of a crucible underneath a layer of cryolite. Some results were published previously (18). The melt was stirred and the dissolution process was followed by use of the alumina probe mentioned above. This experimental procedure involves some problems. The start-up of experiments with two fluid layers is difficult. Model experiments in water showed that stirring of the liquid above the sludge tends to whirl up alumina grains from the sludge. The exposed surface area then becomes ill-defined.

One solution to this problem is to press the alumina into tablets, as was first done by Gerlach et al. (11). In the present work the alumina was mixed with 5 wt % cryolite and an organic binder before pressing and sintering at 1200°C. These tablets retained their shape during the dissolution process. Fig. 5 shows a dissolution curve for an alumina tablet in a stirred melt. The rate of dissolution increased with increasing stirring rate.

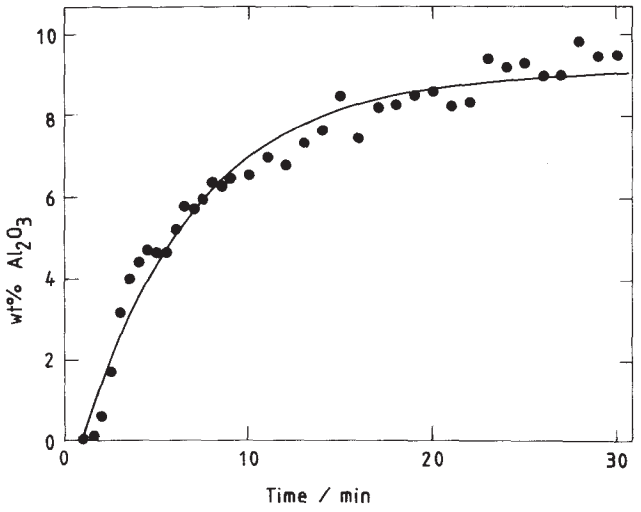

Fig. 5 - Dissolution of a pressed tablet of alumina in molten cryolite at 1025°C. Stirring by impeller, 18 mm dia., 10 mm above the tablet, 325 rpm.

The curve in Fig 5 is fitted to an equation for a mass transfer controlled process

$$r = \frac{dc}{dt} \cdot V = A \cdot k \, (c_{sat} - c) \qquad (7)$$

where V is the volume of bath, A is the surface area of the alumina tablet and k is the mass transfer coefficient. Upon integration the equation becomes

$$c = c_{sat} \, (1 - \exp \, (- \frac{kA}{V} \, t)) \qquad (8)$$

Some corrections must be introduced to this simple equation because the starting point (c = 0, t = 0) is not well defined.

Similar curves were obtained for dissolution of sludge samples, but the rates were higher. One reason for this will be the whirling up of alumina grains from the sludge as mentioned above. Some dissolution rates are given in Table I together with comparable literature data. The agreement is satisfactory for this type of measurements where the results are very dependent upon the experimental condition.

Table I. Rate of Dissolution in g $Al_2O_3/cm^2 \cdot min$ of Alumina which Rests at the Bottom of a Crucible under a Stirred Cryolite Melt at 1025°C.

	Stirring rpm	g Al_2O_3 / $cm^2 \cdot min$	Ref.
Pressed tablet, a-Al_2O_3	200	0.11	Gerlach et
" " , γ-Al_2O_3	200	0.16	al. (11)
Sludge	39	0.086	This work
Pressed tablet	39	0.035	" "
" "	325	0.10	" "
Sinter-corundum	325	0.040	" "

Dissolution of Alumina Added Batchwise

The melt was kept in a graphite crucible (57 mm ID) and moderate stirring was applied (impeller, 18 mm dia. 200 rpm). The purpose of the experiments was to have conditions which are not radically different from conditions during alumina feeding in industrial cells.

After addition the alumina (1-2 wt %) would rest on top of the melt for a while until it was completely wetted by the melt when it would break apart and sink. In such experiments the dissolution rate is very dependent upon the experimental conditions as explained above. For these particular experiments the dissolution times were of the order of 10 minutes, as shown in Fig. 6. Slower stirring rates gave slower dissolution. Fig. 6 also shows a temperature recording which depicts the sharp temperature drop which occurs upon addition of alumina. A marked temperature drop was also experienced by continuous feeding of alumina. This drop is partly due to heating of the alumina and partly due to the endothermic dissolution process (18). Experiments of this kind cannot be conducted under isothermal conditions.

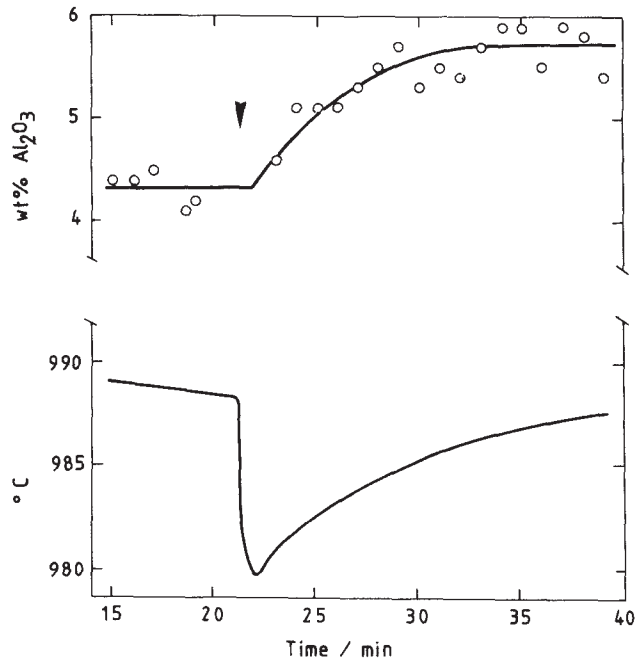

Fig. 6 - Change in alumina content and in bath temperature after addition of 1.5 % alumina (V) to a cryolite-alumina melt. Liquidus temperature before addition: 982°C.

CONCLUSIONS

Dissolution of alumina in the form of stationary sludge or tablets or a rotating disc can be treated as a mass transfer controlled process. The same is probably true also for dispersed powder, but reaction control cannot be ruled out in this case. Heat transfer governs the heating of the alumina up to the bath temperature, but it does not seem to be a limiting factor during dissolution.

For agglomerated alumina powder which is moved by the bath the rate control of the dissolution process is still obscure. The exposed surface area which depends on the extent of agglomeration is probably the most important parameter.

Acknowledgement

The present work was supported by the Royal Norwegian Council for Scientific and Industrial Research and the Norwegian Aluminium Industry.

REFERENCES

1. R. K. Jain, S. B. Tricklebank, B. J. Welch and D. J. Williams, "Interaction of Aluminas with Aluminium Smelting Electrolytes", Light Metals 1983, 609-622.

2. A. S. Bagshaw, G. Kuschel, M. P. Taylor, S. B. Tricklebank and B. J. Welch, "Effect of Operating Conditions on the Dissolution of Primary and Secondary Alumina Powders in Electrolysis", Light Metals 1985, 649-659.

3. Y. Bertaud and A. Lectard, "Aluminum Pechiney Specifications for Optimising the Aluminas Used in Sidebreak and Point Feeding Reduction Pots", Light Metals 1984, 667-686.

4. R. Oedegaard, S. Roenning, S. Rolseth and J. Thonstad, "On Alumina Phase Transformation and Crust Formation in Aluminum Cells", Light Metals 1985, 695-709.

5. R. B. Bird, W. E. Steward, and E. N. Lightfoot, Transport Phenomena, (New York, NY: John Wiley & Sons, Inc., 1960) p. 647, 409.

6. O. A. Asbjørnsen and J. A. Andersen, "Kinetics and Transport Processes in the Dissolution of Aluminium Oxide in Cryolite Melts", Light Metals 1977, Vol. 1., 137-152.

7. R. K. Jain, M. P. Taylor, S. B. Tricklebank and B. J. Welch, "A Study of the Relationship Between the Properties of Alumina and Its Interaction with Aluminium Smelting Electrolytes", Proc. 1st Int. Symp. on Molten Salt Chem. and Tech., Kyoto, Japan, 1983, p. 59.

8. M. P. Taylor, B. J. Welch and R. McCibbin, "Effect of Convective Heat Transfer and Phase Change on the Stability of Aluminium Smelting Cells", paper presented at the AIChE Annual Meeting, San Francisco, 25-30 Nov. 1984.

9. J. Thonstad, "Aluminium Electrolysis, Electrolyte and Electrochemistry", in Advances in Molten Salt Chemistry, Vol. 6, ed. G. Mamantov, C. B. Mamantov and J. Braunstein, Elsevier, Amsterdam 1987, 73-126.

10. J. Thonstad, F. Nordmo and J. B. Paulsen, "Dissolution of Alumina in Molten Cryolite", Met. Trans. (1972) 403-408.

11. J. Gerlach, U. Hennig and K. Kern, "The Dissolution of Aluminum Oxide in Cryolite Melts", Met. Trnas. 6B (1975) 83-86.

12. P. M. Shurygin, V. N. Boronenkov and V. I. Kryuk, Isv. Vyssh. Uchebn. Zav. Tsvet. Met. 5 (3) (1962) 59-66. Ibid. 5 (4) 1962, 59-66.

13. P. Desclaux and M. Rolin, "Etude de coefficient de diffusion de l'alumine dans les melanges cryolithe-alumine", Rev. Int. Hautes Temp. et Refract. 8 (1971) 227-236.

14. J. Gerlach, U. Hennig and H. D. Pötsch, "Zur Auflösungskinetik von Aluminiuimoxid in Kryolithschemlzen mit Zusätzen von Al_2O_3, AlF_3, CaF_2, LiF oder MgF_2. Erzmetall, 31 (1978) 496-504.

15. V. G. Levich, Physical Hydrodynamics. (Englewood Cliffs, N. J., Prentice Hall, Inc., 1962), pp. 60-72.

16. K. Grjotheim, C. Krohn, M. Malinovsky, K. Matiasovsky and J. Thonstad, Aluminium Electrolysis. Fundamentals of the Hall-Heroult Process. (Aluminium-Verlag, Düsseldorf 1982) 181-182.

17. J. Thonstad, "Semicontinuous Determination of the Concentration of Alumina in the Electrolyte of Aluminum Cells", Met. Trans. 8B (1977) 125-130.

18. J. Thonstad, P. Johansen and E. W. Kristensen, "Some Properties of Alumina Sludge", Light Metals 1980, 227-239.

APPENDIX. HEAT AND MASS TRANSFER TO A SINGLE ALUMINA PARTICLE.

Mass Transfer and Time of Dissolution

Equations concerning forced convection mass transfer between fluid and a solid body are usually given as a correlation between the dimensionless Sherwood, Reynolds and Schmidt numbers. For a sphere, the following equation applies (5) (all symbols are explained in Table A2)

$$Sh = 2 + 0.6\ Re^{1/2}\ Sc^{1/3} \qquad (A1)$$

or

$$k \cdot d_p/D = 2 + 0.6\ (\varrho v d_p/\mu)^{1/2}\ (\mu/\varrho\ D)^{1/3} \qquad (A2)$$

The terminal velocity of a single alumina particle falling through a cryolite melt can be calculated by Stokes law

$$v = d_p^{\,2} \cdot g\ (\varrho_p - \varrho)/18 \cdot \mu \qquad (A3)$$

provided that $Re < 2$. Table AI gives the Reynolds number and the Sherwood number for different particle diameters, calculated with physical data taken from Table AII.

Table AI. Reynolds Number and Sherwood Number for Different Particle Diameters

$d_p \cdot 10^6$/m	Re	Sh
0	0	2
5	$1.48 \cdot 10^{-5}$	2.02
10	$1.18 \cdot 10^{-4}$	2.06
20	$9.44 \cdot 10^{-4}$	2.18
50	$1.48 \cdot 10^{-2}$	2.72
100	0.118	4.04

The mass of alumina in the particle is

$$m = \pi \cdot d_p^3 \cdot \varrho_a/6 \qquad (A4)$$

and the flux of alumina from the surface to the bulk of the melt

$$dm/dt = k \cdot (c_{sat} - c) \cdot \pi d \qquad (A5)$$

Differentiation of eq. (A4) and combination with (A5) gives upon integration

$$t = \int_{dp}^{0} - [\varrho_a/2k\ (c_{sat} - c)]\ d(d_p) \qquad (A6)$$

Eq. (A6) must be integrated numerically, since k is a complex function of the diameter (see eq. (A2)). However, the Sherwood number apporaches a contant value at small Reynolds numbers. When Sh = 2, eq. (A6) can readily be integrated to give the maximum time of dissolution

$$t = \varrho_a \cdot d_p^2/8D\ (c_{sat} - c) \qquad (A7)$$

Taking the concentration difference to be 100 kg/m^3 (4.9 wt %) and other data from Table A2, the maximum time of dissolution becomes 4.1 s for a particle with diameter 50 μm.

Combined Heat and Mass Transfer

In the example above, it was implicitly assumed that the dissolution is purely diffusion controlled. However, since the heat of dissolution is relatively large, it has been suggested that the process may be heat transfer controlled. Heat transfer to a sphere can be correlated by an equation similar to eq. (A1),

$$Nu = 2 + 0.6\ Re^{1/2}\ Pr^{1/3} \qquad (A8)$$

or

$$h \cdot d_p/\lambda = 2 + 0.6\ (\varrho v d_p/\mu)^{1/2}\ (C_p \cdot \mu/\lambda)^{1/3} \qquad (A9)$$

At very small Reynolds numbers,

$$Nu/Sh = hD/\lambda k = 1 \qquad (A10)$$

whereas for large Re (and non-spherical geometries)

$$Nu/Sh = (Pr/Sc)^{1/3} = (C_p \cdot \varrho \cdot D/\lambda)^{1/3} = 0.22 \qquad (A11)$$

Using data from Table A2, we obtain $h/k = 3.33 \cdot 10^8$ for small Re and $0.73 \cdot 10^8$ for high Re. The ratio between the heat flux and the mass flux corresponds to the heat of dissolution, which increases with decreasing alumina concentration (see Table A2)

$$Q/J = h \cdot (T - T^*)/k\ (c_{sat} - c) = \Delta H_d \qquad (A12)$$

We may select a medium value for the heat of dissolution (ΔH_d = 1500 $kJ \cdot kg^{-1}$). When the concentration difference is 100 $kg \cdot m^{-3}$, the temperature difference between the alumina surface and the bulk of the melt becomes 2.2 degrees at low Reynolds numbers, and 0.5 degrees at high Reynolds numbers or non-spherical geometries.

Table II. Nomenclature and assumed physical constants.

Symbol	Definition	Dimension/ Assumed value (1000^0C)
c	Alumina conc., bulk of melt	$kg \cdot m^{-3}$
c_{sat}	Alumina conc. at particle	$kg \cdot m^{-3}$
C_p	Heat capacity of melt	1850 $J \cdot kg^{-1}\ K^{-1}$
D	Diffusion coeff., alumina	$1.5 \cdot 10^{-9}\ m^2 \cdot s^{-1}$
d_p	Particle diameter	m
g	Acceleration of gravity	9.82 $m \cdot s^{-2}$
h	Heat transfer coefficient	$W \cdot m^{-2} \cdot K^{-1}$
ΔH_d	Heat of dissolution	820-2750 $kJ \cdot kg^{-1}$
J	Flux of alumina	$kg \cdot s^{-1}$
k	Mass transfer coefficient	$m \cdot s^{-1}$
m	Mass of alumina particle	kg
Q	Heat flux	W
t	Time of dissolution	s
T	Melt temperature	K
T*	Temp. at particle surface	K
v	Terminal velocity	$m \cdot s^{-1}$
λ	Thermal conductivity of melt	0.5 $W \cdot m^{-1} \cdot K^{-1}$
μ	Dynamic viscosity	$3 \cdot 10^{-3}\ kg \cdot m^{-1} \cdot s^1$
ϱ_a	Density of particle, in air	1975 $kg \cdot m^{-3}$
ϱ	Density of melt	2050 $kg \cdot m^{-3}$
ϱ_p	Density of particle, in melt	2975 $kg \cdot m^{-3}$
Nu	Nusselt number, hdp/λ	-
Pr	Prandtl number, $C_p \cdot \mu/\lambda$	11.1
Re	Reynolds number, $\varrho v d_p/\mu$	-
Sc	Schmidt number, μ/ϱD	976
Sh	Sherwood number, kd_p/D	-